Stromal response to Hedgehog signaling restrains pancreatic cancer progression

John J. Lee[a,b,1], Rushika M. Perera[c,1], Huaijun Wang[d,2], Dai-Chen Wu[a,2], X. Shawn Liu[a,2], Shiwei Han[e], Julien Fitamant[c], Phillip D. Jones[a], Krishna S. Ghanta[c], Sally Kawano[a], Julia M. Nagle[c], Vikram Deshpande[c], Yves Boucher[e], Tomoyo Kato[f], James K. Chen[f], Jürgen K. Willmann[d], Nabeel Bardeesy[c,3], and Philip A. Beachy[a,g,h,3]

[a]Institute for Stem Cell Biology and Regenerative Medicine, [b]Division of Oncology, Department of Medicine, [g]Department of Biochemistry, [f]Department of Chemical and Systems Biology, and [d]Molecular Imaging Program, Department of Radiology, Stanford University School of Medicine, Stanford, CA 94305; [c]Cancer Center, Massachusetts General Hospital and Harvard Medical School, Boston, MA 02114; [e]Edwin L. Steele Laboratory, Department of Radiation Oncology, Massachusetts General Hospital and Harvard Medical School, Boston, MA 02114; and [h]Howard Hughes Medical Institute, Stanford, CA 94305

Contributed by Philip A. Beachy, June 23, 2014 (sent for review May 27, 2014; reviewed by Brian Lewis and Anirban Maitra)

Pancreatic ductal adenocarcinoma (PDA) is the most lethal of common human malignancies, with no truly effective therapies for advanced disease. Preclinical studies have suggested a therapeutic benefit of targeting the Hedgehog (Hh) signaling pathway, which is activated throughout the course of PDA progression by expression of Hh ligands in the neoplastic epithelium and paracrine response in the stromal fibroblasts. Clinical trials to test this possibility, however, have yielded disappointing results. To further investigate the role of Hh signaling in the formation of PDA and its precursor lesion, pancreatic intraepithelial neoplasia (PanIN), we examined the effects of genetic or pharmacologic inhibition of Hh pathway activity in three distinct genetically engineered mouse models and found that Hh pathway inhibition accelerates rather than delays progression of oncogenic Kras-driven disease. Notably, pharmacologic inhibition of Hh pathway activity affected the balance between epithelial and stromal elements, suppressing stromal desmoplasia but also causing accelerated growth of the PanIN epithelium. In striking contrast, pathway activation using a small molecule agonist caused stromal hyperplasia and reduced epithelial proliferation. These results indicate that stromal response to Hh signaling is protective against PDA and that pharmacologic activation of pathway response can slow tumorigenesis. Our results provide evidence for a restraining role of stroma in PDA progression, suggesting an explanation for the failure of Hh inhibitors in clinical trials and pointing to the possibility of a novel type of therapeutic intervention.

tumor stroma | cancer therapy | *Sonic hedgehog* | hedgehog agonist | cerulein

Pancreatic ductal adenocarcinoma (PDA) is the fourth most common cause of cancer-related death in the United States and is the most lethal of common human malignancies, with a 5-y survival rate of ∼7% (1, 2). The most effective chemotherapy regimens for metastatic or locally advanced inoperable disease are largely palliative and are capable of extending overall survival by only several months (3, 4). Even localized disease, treatable with surgery followed by adjuvant chemotherapy, has a dismal 5-y survival rate of 24% (1). Among gastrointestinal malignancies, PDA is unique in that it is predominantly driven by oncogenic Kras activity. In addition, PDA pathogenesis is marked by a striking desmoplastic reaction to invading tumor cells. This desmoplasia includes a dense extracellular matrix with abundant stromal fibroblasts and influences the cellular biology of the tumor as well as its response to chemotherapeutic agents.

Hedgehog (Hh) signaling has been thought to play a role in PDA desmoplasia and tumor progression but is notable during embryonic development of the pancreas for its absence in the region of embryonic endoderm from which the pancreas forms (5–7). This absence of activity is required for normal specification of early pancreatic progenitor fate, and pharmacologic or antibody treatments that inhibit Hh pathway signaling cause expansion of such fates, as indicated by ectopic expression of the pancreatic progenitor marker *Pdx1* (5–7). In adult mice, expression of *Shh* (*Sonic hedgehog*) is barely detectable and is limited to pancreatic duct glands, which are small outpouchings of the major pancreatic ducts (8).

Increased levels of *Shh* expression are observed in the setting of pancreatic injury and throughout the course of human and murine PDA progression, beginning in the early epithelial precursor lesions, acinar-ductal metaplasia (ADM) and pancreatic intraepithelial neoplasia (PanIN). *Shh* is also expressed in locally invasive carcinomas and in distant metastases (9–11). Pharmacologic blockade of Hh pathway response with antagonists, such as cyclopamine and HhAntag, that inhibit activity of the critical Hh-transducing molecule Smoothened (Smo) has been reported to reduce the growth of human pancreatic cancer xenografts in nude mice (9, 11, 12); cyclopamine was also reported to prolong survival in a genetically engineered mouse (GEM) model of pancreatic cancer (13). Hh pathway blockade using either small-molecule antagonists or the Shh ligand-blocking antibody 5E1 was also

Significance

Preclinical studies have suggested that Hedgehog (Hh) pathway inhibition reduces growth and metastasis of pancreatic ductal adenocarcinoma (PDA), but ensuing clinical trials of Hh pathway antagonists combined with cytotoxic chemotherapy have not succeeded. Here, we find in three distinct genetically engineered mouse models that genetic and pharmacologic inhibition of Hh pathway activity actually accelerates PDA progression. Furthermore, we find that the acute modulation of pathway activity regulates the balance between epithelial and stromal elements, with inhibition causing suppression of desmoplasia and accelerated growth of epithelial elements and activation causing stromal hyperplasia and reduced growth of the neoplastic epithelium. Our study explains previous clinical trial results and suggests the possibility of novel types of therapeutic interventions.

Author contributions: J.J.L., R.M.P., Y.B., J.K.W., N.B., and P.A.B. designed research; J.J.L., R.M.P., H.W., D.-C.W., X.S.L., S.H., J.F., P.D.J., K.S.G., S.K., J.M.N., and V.D. performed research; T.K. and J.K.C. contributed new reagents/analytic tools; J.J.L., R.M.P., H.W., S.H., J.F., V.D., N.B., and P.A.B. analyzed data; and J.J.L., R.M.P., N.B., and P.A.B. wrote the paper.

Reviewers: B.L., University of Massachusetts Medical School; and A.M., University of Texas MD Anderson Cancer Center.

The authors declare no conflict of interest.

[1]J.J.L. and R.M.P. contributed equally to this work.

[2]H.W., D.-C.W., and X.S.L. contributed equally to this work.

[3]To whom correspondence may be addressed. Email: pbeachy@stanford.edu or Bardeesy.Nabeel@mgh.harvard.edu.

This article contains supporting information online at www.pnas.org/lookup/suppl/doi:10.1073/pnas.1411679111/-/DCSupplemental.

reported to inhibit distant metastases from human pancreatic xenografts in athymic nude mice (14–16).

Hh signaling in normal pancreas and in PDA is exclusively paracrine (17), with expression of *Shh* limited to epithelium and response restricted to stroma. Correspondingly, deletion of Smo in the pancreatic epithelium does not affect PDA pathogenesis in a GEM model (18). Hh response and its inhibition thus primarily affect stromal cells and, in the setting of PDA, has been reported to have a major impact on the desmoplastic reaction (19–21). An indirect therapeutic benefit of Hh pathway blockade thus may be to decrease stromal fibrosis and increase functional vascularity, potentially enhancing the penetration and effectiveness of standard chemotherapy (20).

Given the preclinical evidence suggesting possible therapeutic benefits of Hh pathway blockade in limiting local or metastatic PDA growth and enhancement of chemotherapy, several clinical trials have been launched using small-molecule Hh pathway antagonists for this disease (22). These trials have typically combined an Hh pathway antagonist with standard chemotherapy, but, unfortunately, results have been either negative or equivocal. Thus, for example, in a phase 2 double-blind placebo-controlled study of saridegib, a cyclopamine derivative, 122 patients with previously untreated metastatic PDA were treated with either saridegib plus gemcitabine or placebo plus gemcitabine, with overall survival (OS) as a primary end point. Interim data analysis indicated that median OS for the saridegib plus gemcitabine arm was less than 6 mo whereas the median OS for the placebo plus gemcitabine arm was greater than 6 mo, resulting in termination of the clinical trial (23). In another randomized, placebo-controlled phase 2 study, the FDA-approved Smo antagonist vismodegib plus gemcitabine was compared with placebo plus gemcitabine in patients with previously untreated metastatic PDA (24). At the time of interim analysis, the OS was 6.3 versus 5.4 mo for vismodegib versus the placebo arm, with an unimpressive hazard ratio of 0.97. Recently, an interim analysis was reported of a single-arm phase 2 study using vismodegib in combination with gemcitabine and nab-paclitaxel (25), with an estimated OS of 10 mo for 59 patients, which is greater than the published historic controls of 8.5 mo for gemcitabine plus nab-paclitaxel (4).

Results

Genetic Reduction of Hh Signaling Accelerates Growth of PDA Lesions. To gain further insights into the cellular effects of Hh signaling in PDA and a more precise understanding of human clinical trial data, we initiated a series of studies modulating the pathway in GEM models. First, we assessed the impact of genetic inactivation of Shh (using $Shh^{fl/fl}$ mice) on formation of premalignant PanIN and subsequent PDA progression in the context of the *Ptf1a-Cre:LSL-Kras*^{G12D} (KC) model (26). *Ptf1a-Cre:Shh*$^{fl/fl}$ and *Ptf1a-Cre:Kras*^{G12D}*:Shh*$^{fl/fl}$ (KCS) mice were born at the expected frequency and showed no abnormalities in pancreatic development (Fig. S1). Thus, Shh is dispensable for normal pancreatic development irrespective of Kras status.

KC mice develop focal PanIN lesions by ∼1–2 mo of age, and these lesions increase in number and grade, eventually progressing to invasive PDA (mean latency >16 mo) (26). To determine the effect of Shh deletion on PanIN formation, we euthanized experimental mice and controls at 6 mo of age. At this time point, KC animals (n = 21) exhibited PanIN lesions (mostly PanIN-1A) that occupied on average 21.3 ± 18.2% of the total pancreas (Fig. 1 *A* and *B*). Unexpectedly, KCS mice (n = 38) showed a significant increase in PanIN burden compared with KC controls, with an average of 37.4 ± 27.3% of pancreatic area comprising PanIN lesions ($P < 0.02$) (Fig. 1*A*) and with a greater proportion of higher-grade lesions (6.6 ± 5.3 PanIN-2/3 lesions per section in KCS mice compared with 1.3 ± 1.4 in KC controls; $P < 0.001$) (Fig. 1*B*, *Right*). There was a corresponding threefold increase in proliferating ($PCNA^+$) epithelial cells within PanIN lesions (Fig. 1 *C* and *D*); *Shh* deletion in the pancreatic epithelium thus enhances the formation and proliferation of $Kras^{G12D}$-driven PanIN lesions.

Short-term treatment of mice with the cholecystokinin analog cerulein results in an acute pancreatitis phenotype characterized by acinar cell death and inflammation and transient dedifferentiation of acinar cells to duct-like structures [acinar-to-ductal metaplasia (ADM), accompanied by expression of *Sox9*], followed by restoration of normal pancreatic architecture over a period of 1 wk (27). In the context of activated Kras, regeneration is suppressed, and there is a pronounced acceleration of PanIN formation arising from the ADM lesions (28, 29). In addition, Shh expression is induced upon cerulein treatment, and pharmacologic inhibition of the Hh pathway impairs recovery from cerulein-induced injury, characterized by persistence of undifferentiated ADM lesions staining positive for progenitor cell markers (30). Based on these observations and the data just presented, we predicted that Shh deletion would strongly synergize with cerulein treatment to drive PanIN formation in the $Kras^{G12D}$-expressing pancreas. We exposed 8-wk-old mice to acute cerulein treatment and harvested the pancreata after one month of recovery. Knockout of Shh greatly enhanced $Kras^{G12D}$-driven PanIN formation, leading to virtually complete replacement of the normal exocrine pancreas with ductal structures and fibrosis (occupying 78 ± 25% of the KCS pancreas compared with 39 ± 25% in KC controls; $P < 0.03$) (Fig. 1 *E* and *F*). Consistent with an ongoing expansion of ADM lesions that have failed to undergo redifferentiation, the remaining acinar cells in KCS pancreata showed an approximately threefold increase in the percentage staining positive for Sox9, a marker of developmental plasticity required for reprogramming of acinar cells to a more duct cell-like PanIN phenotype (Fig. 1 *G* and *H*) (28). These data indicate that Shh signaling normally promotes epithelial differentiation and suppresses Kras-dependent neoplasia in the pancreas, with its loss accelerating spontaneous and pancreatitis-induced PanIN formation.

We monitored an additional cohort of animals up to age 55 wk and then performed necropsies to determine whether Shh status influences the development of advanced PanIN and invasive PDA. Notably, 2 of 11 KCS mice exhibited signs of illness and palpable pancreatic masses at 38 wk of age requiring sacrifice, which revealed metastatic PDA, whereas all of the KC animals (n = 13) appeared healthy throughout the observation period. Moreover, histopathologic analysis revealed that the proportion of neoplastic to normal pancreatic tissue was greatly increased in KCS mice compared with KC controls at 55 wk (88.6 ± 13.4% versus 17.7 ±16.8%, respectively; $P < 0.001$) (Fig. 2 *A* and *B*). Notably, a fivefold increase in the number of high-grade PanINs in KCS mice compared with KC controls was also observed (14.9 ± 5.5 versus 3 ± 3.2; $P < 0.001$)—along with a sixfold increase in the size of PDA lesions (Fig. 2*B*). Thus, Shh deficiency accelerates both PanIN initiation as well as progression to PDA.

Genetic Reduction of Hh Signaling in Murine PDA Decreases Survival. The tumor suppressor p53 is inactivated in the majority of human PDA, and heterozygous inactivation of p53 greatly reduces the latency of Kras-driven PDA in the *Ptf1a-Cre:Kras*^{G12D}*:p53*$^{fl/+}$ (KPC) model. We crossed the $Shh^{fl/fl}$ allele into this model (generating KPCS mice) to examine the impact of Shh deficiency on PDA phenotypes in the context of a highly tumor-prone setting. Shh deficiency again accelerated PDA formation, with KPCS mice surviving a mean of 18.8 ± 4.8 wk compared with 22.9 ± 5.6 wk in KPC controls ($P < 0.015$) (Fig. 2*C*). Moreover, Shh-deficient PDA exhibited a significant increase in vessel density compared with the tumors with Shh intact, as revealed by

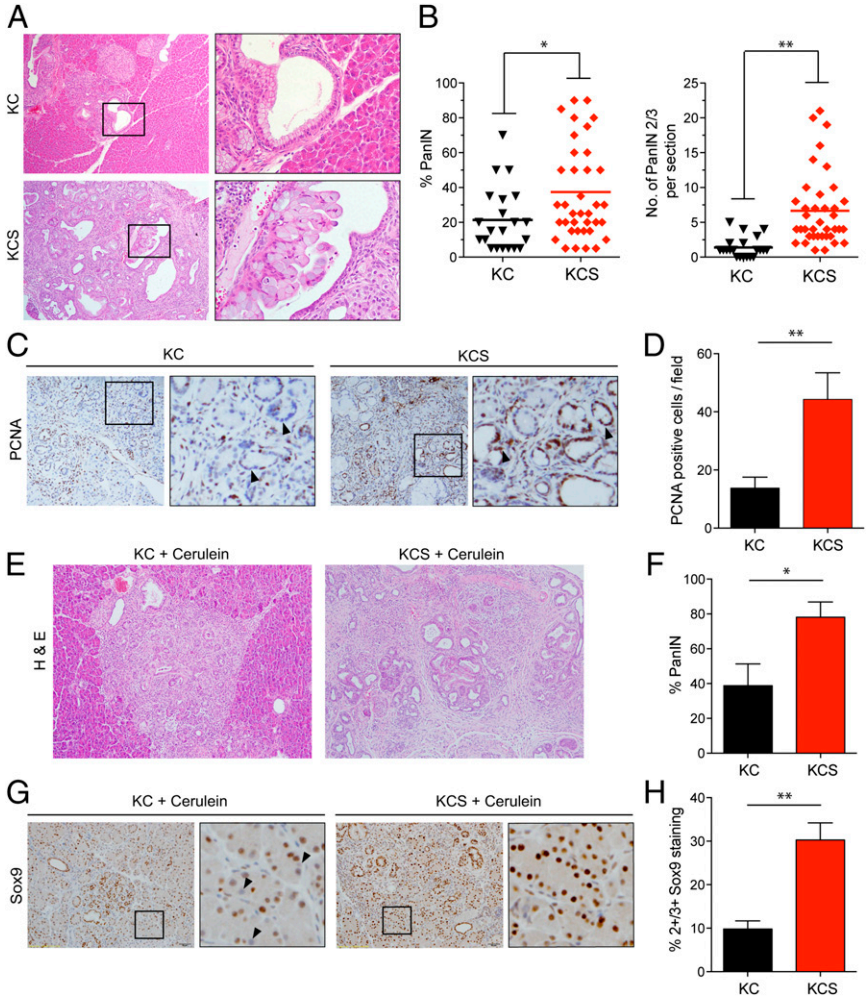

Fig. 1. Accelerated PanIN formation following *Shh* loss. (*A–D*) Analysis of pancreata from KC and KCS mice euthanized at 6 mo of age. (*A*) Representative histologic images. The boxed regions show PanIN-1A lesions in a KC mouse (*Upper*) and PanIN-2 in a KCS mouse (*Lower*). (*B*) Quantification of percentage of pancreas occupied by PanIN (*Left*), and number of high-grade PanIN-2/3 lesions per section (*Right*); $*P < 0.02$; $**P < 0.001$. The line indicates the mean value. (*C*) Immunohistochemistry for PCNA. Boxed regions are magnified at *Right*. Arrowheads indicate negatively and positively stained nuclei of ductal epithelial cells from KC mice (*Left*) and KCS mice (*Right*), respectively. (*D*) The number of PCNA-positive cells per field ($n = 10$), from a total of five mice per group was quantified; $*P < 0.01$. Error bars indicate SEM. (*E–H*) Eight-week-old KC ($n = 4$) and KCS ($n = 8$) mice were treated with cerulein (six hourly injections per day for two consecutive days), and pancreata were collected 1 mo later. (*E*) Representative histology. (*F*) Quantification of percentage of PanIN; $*P < 0.03$. (*G*) Immunohistochemistry for Sox9 (boxed region magnified at *Right*; arrowheads indicate negatively stained nuclei in a KC mouse pancreas). (*H*) Quantification of Sox9 staining (four mice per group, 10 high-power fields (hpfs) per pancreas). The percentage of nuclei scoring as 2+/3+ in staining intensity is plotted. Error bars indicate SEM; $**P < 0.001$.

Meca32 staining ($P < 0.035$) (Fig. 2*D*). As in early PanIN lesions, Shh deficiency was associated with an increase in proliferation of the neoplastic epithelium in advanced PDA (Fig. 2*E*). *Shh* function thus restrains PanIN initiation and progression to PDA, in the context of an aggressive tumor model, and suppresses the formation of the tumor vasculature.

Pharmacologic Reduction of Hh Signaling Decreases Survival and Accelerates Tumor Growth in Murine PDA. In the genetic studies presented above, Shh was inactivated in pancreatic epithelial lineages during embryogenesis. The acceleration of $Kras^{G12D}$-driven PDA that we observed thus could reflect alterations in the differentiation of pancreatic progenitor cells during development, especially as absence of pathway activity during development increases progenitor phenotype (5, 31). To address more directly the impact of Hh signaling loss on tumorigenesis, we subjected adult PDA-prone mice to sustained treatment with the Hh pathway antagonist vismodegib to block the effects of Shh produced by epithelial cells on surrounding responding cells. We used a previously described mouse model for PDA that carries coincident Kras and Ink4a/Arf mutations (32), as seen in >80% of human PDA, and integrated the *Gli1-nLacZ* knock-in reporter allele (33). The presence of both Kras and Ink4a/Arf mutations in this KICG model ($Kras^{LSL\text{-}G12D/+}$; $Ink4a/Arf^{-/-}$; *Pdx1-cre*; $Gli1^{nLacZ/+}$) greatly accelerates PDA development, with morbidity and death typically occurring before 11 wk (32); in addition, LacZ expression under control of the Hh-responsive *Gli1* promoter enables us to reliably localize Hh-responsive cells.

KICG mice were treated either with vismodegib (100 mg/kg daily) or vehicle control starting at 5 wk of age, at which point the animals harbored high grade PanINs and established PDA. We confirmed that vismodegib treatment significantly reduced Hh response in the mouse pancreas (Fig. S2*A*). Consistent with our genetic studies, vismodegib treatment significantly reduced survival (7.71 wk compared with 8.86 wk for control animals; $P = 0.019$) (Fig. 2*F*).

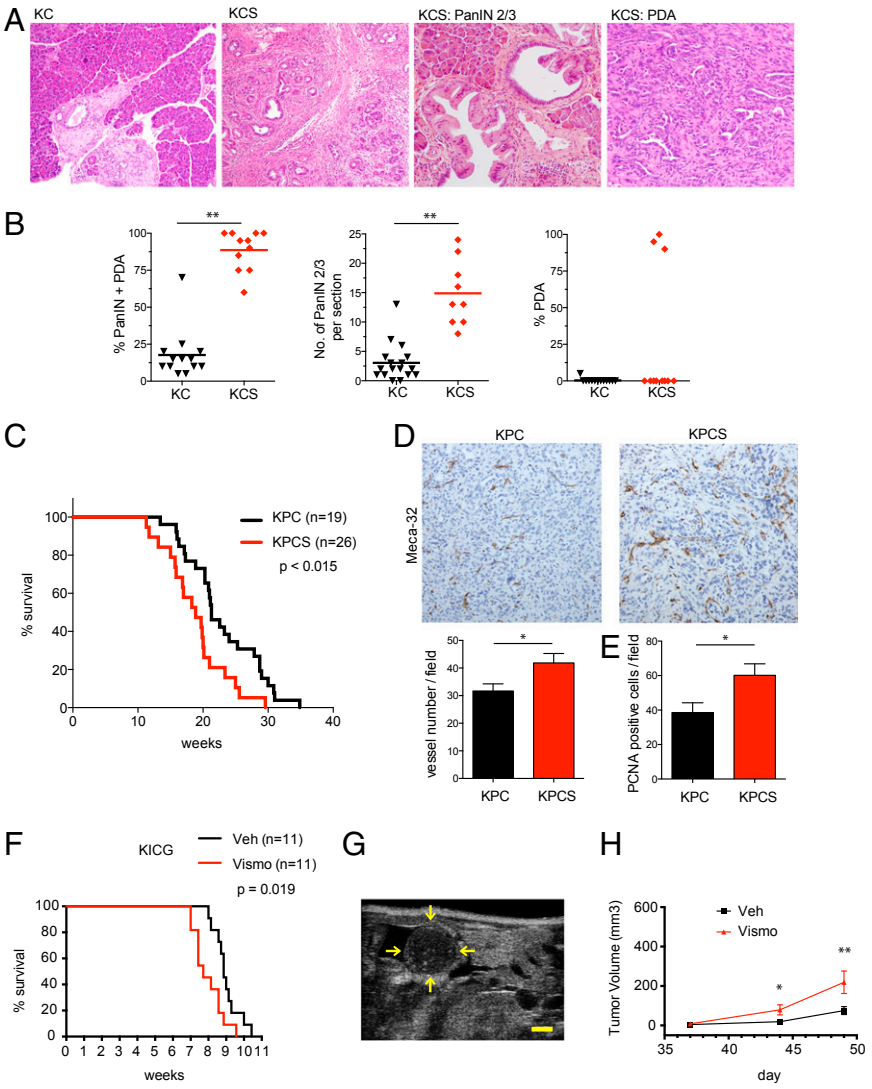

Fig. 2. Loss of Hh response promotes PDA development. (*A and B*) KC and KCS mice were euthanized at age 55 wk. (*A*) Representative histology of pancreata. (*B*) Quantification of percentage of PanIN and PDA (*Left*), number of high-grade PanIN2/3 (*Center*), and percentage of PDA (*Right*) in aged KC ($n = 13$) and KCS ($n = 11$) mice. The line indicates the mean value. $^{**}P < 0.001$. (*C–E*) KPC and KPCS mice were euthanized upon signs of illness (*Materials and Methods*). (*C*) Kaplan–Meier analysis showing time to euthanization. All animals had verified PDA. (*D*) Immunohistochemistry for Meca32; chart (*Lower*) shows quantification of staining from 10 hpf from five pancreata per group; $^{*}P < 0.035$. Error bars indicate SEM. (*E*) Immunohistochemistry for PCNA reveals increased proliferation in KPCS pancreata compared with KPC control mice; $^{*}P < 0.03$. Error bars indicate SEM. (*F*) Kaplan–Meier analysis demonstrates that vismodegib treatment (red) starting on day 35 decreases survival in KICG mice compared with vehicle (black). (*G*) Transverse B-mode ultrasound image of a representative 2.5-mm pancreatic cancer focus in the body/tail region of the pancreas. The yellow arrows denote outline of the tumor surface. (Scale bar: 1 mm.) (*H*) Vismodegib treatment starting on day 35 accelerates growth of tumors as measured by ultrasound imaging. Total volumes of tumors detected per mouse in each treatment group are shown. A significant difference in median tumor size was measured on day 44 ($^{*}P = 0.029$; $n = 16$ per group) and was further increased by day 49 ($^{**}P = 0.027$; $n = 12$). There was no significant difference on day 37 ($P = 0.296$; $n = 16$ per group). Error bars indicate SEM.

To determine whether accelerated demise in animals with impaired Hh signaling is associated with more rapid tumor growth, we used B-mode ultrasound live imaging (Fig. 2*G*) (34, 35) to measure and track tumor size within pancreata of KICG mice. We found that overall tumor volumes in KICG mice treated with vismodegib (100 mg/kg daily) beginning at 35 d had significantly increased by day 44 compared with vehicle-treated animals (Fig. 2*H*) ($P = 0.029$, $n = 16$ per group), with a further increase by day 49 (Fig. 2*H*) ($P = 0.027$; $n = 12$ per group). Taken together, these tumor growth and host survival data demonstrate that pharmacologic Hh pathway inhibition significantly accelerates the course of established PDA, even in a highly aggressive murine model that carries coincident Kras and Ink4a/Arf mutations.

Experimental Strategy for Analysis of Hh Pathway Activity in PDA Development. We have noted an acceleration of disease progression by either genetic or pharmacologic Hh pathway blockade in three distinct murine models of PDA. We do not know, however, how direct the effects of pathway inhibition are in these models, as they occurred over periods of many weeks or months. To more directly monitor and understand the role of Hh signaling, we extended our pharmacologic analysis to include Hh pathway activation as well as inhibition, and we used cerulein treatment to accelerate and synchronize PanIN development. In these experiments, KICG mice at early stages of PanIN development (4 wk of age) were treated throughout an approximately 1-wk period with pharmacologic Hh pathway modulators, with administration of cerulein on two consecutive days at the beginning of the treatment

period (Fig. 3*A*). For pathway inhibition, we used vismodegib and, for activation, we identified the potent Hh pathway agonist SAG21k (36) as an orally available small molecule that causes sustained elevation of Hh response in the mouse pancreas within 4 h of administration (Fig. S2*B*).

Hh Pathway Activity Mediates Hyperplasia of *Gli1*-Expressing Stromal Cells. A striking and immediately apparent effect of Hh pathway modulation in cerulein-treated mice was a shift in the relative balance of epithelial and stromal elements. Considering first the stromal compartment, we found that expression of oncogenic Kras combined with cerulein treatment increased the number of *Gli1*-expressing stromal cells 81-fold (Fig. 3 *B*, *E*, *H*, and *I*) (KICG vs. ICG mice; $P = 0.0001$, $n = 5$ per group; see Fig. S3 for absence of cerulein). Additional treatment with SAG21k to activate the Hh pathway further increased by 3.2-fold the number of these cells (Fig. 3 *E*, *G*, and *I*) ($P < 0.0001$, $n = 6$ per group) whereas Hh pathway inhibition with vismodegib decreased the number of stromal *Gli1*-expressing cells in KICG mice by 40% (Fig. 3 *E*, *F*, and *I*) ($P = 0.063$, $n = 6$ per group). We do not know the source of the additional stromal cells observed upon SAG21k treatment.

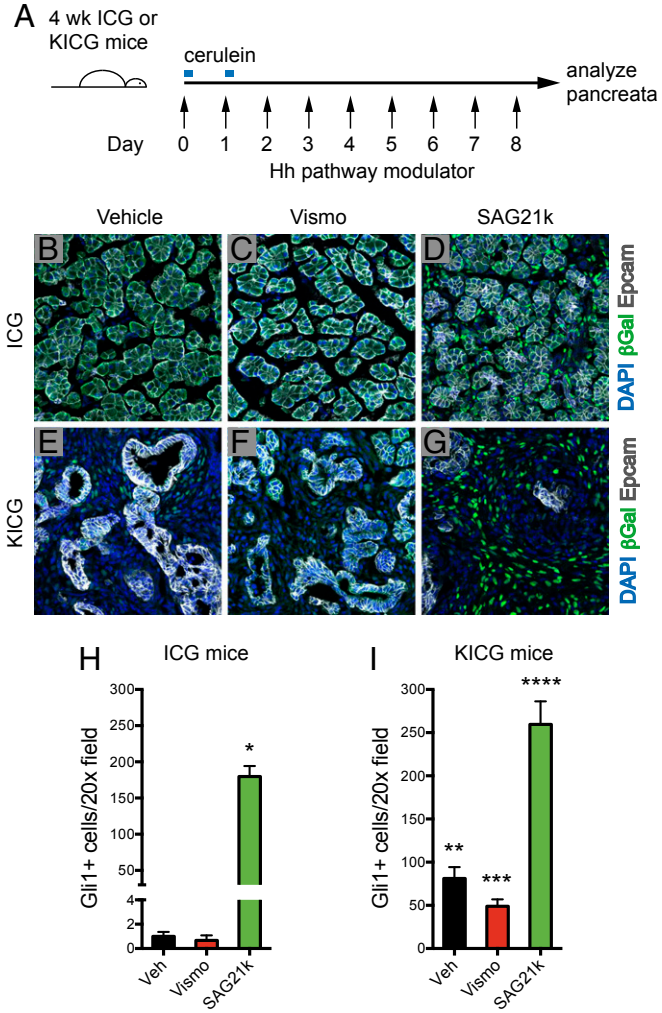

Fig. 3. Hh response augments the number of *Gli1*-expressing stromal cells in cerulein-enhanced oncogenesis. (*A*) Schema for cerulein studies. Four-week-old ICG or KICG were given six hourly doses of cerulein on days 0 and 1. On days 0 through day 8 mice were given either vehicle, vismodegib, or SAG21k. Pancreata were harvested on day 8, 4 h after the last dose of Hh pathway modulating agent. (*B–D* and *H*) ICG mice do not form PanIN lesions in the setting of cerulein-induced pancreatitis. In these animals, vismodegib does not alter significantly the number of *Gli1*$^+$ cells. However, SAG21k increases the amount of *Gli1*$^+$ cells by 180-fold (*$P < 0.0001$, $n = 6$). Error bars indicate SEM. (*E–G* and *I*) In contrast, PanIN lesions are induced in KICG mice, associated with an 81-fold increase in *Gli1*$^+$ cells observed in vehicle-treated KICG mice compared with vehicle-treated ICG controls (**$P = 0.0001$, $n = 6$). Vismodegib resulted in a nonsignificant decrease in *Gli1*$^+$ cells in KICG mice (Vismo vs. Veh in *I*, ***$P = 0.063$, $n = 6$) whereas SAG21k resulted in a prominent increase (SAG21k vs. Veh in *I*, ****$P < 0.0001$, $n = 6$). Error bars indicate SEM.

The increased number of *Gli1*$^+$ stromal cells upon induction by Hh pathway activation is consistent with a known role for Hh signaling in promoting desmoplasia in PDA (19–21); we also noted that SAG21k induced a myofibroblast-like phenotype, marked by increased expression of alpha-Smooth Muscle Actin (αSMA) (Fig. 4 *A* and *C*) (37, 38) and of the extracellular matrix protein Collagen I (Col I) (Fig. 4 *D* and *F*) (39, 40). In contrast, treatment with vismodegib produced a distinct reduction in expression of these proteins (Fig. 4 *B* and *E* vs. Fig. 4 *A* and *D*). We also noted that pathway activation by SAG21k caused accumulation of a zone of cells expressing CD45 surrounding the remaining PanIN lesions (Fig. 4 *G–I*; see *Discussion*).

Epithelial Cell Proliferation and PanIN Formation Can Be Increased or Decreased by Pharmacologic Modulation of Hh Pathway Activity. Although primary response to Hh signaling occurs in stromal cells, pharmacologic modulation of Hh pathway activity also affects the abundance and cellular phenotype of adjacent epithelial elements. Indeed, histological examination with H&E staining of KICG mice treated with cerulein thus showed that 16% of the pancreata analyzed were occupied by PanIN lesions by 5 wk of age (Fig. 5 *A*, *D*, and *G*). Upon additional inhibition of pathway activity by vismodegib, the proportion of pancreata occupied by PanIN lesions doubled to 37% (Fig. 5 *B*, *E*, and *G*) ($P = 0.016$, $n = 4$ per group) whereas pathway activation by SAG21k dramatically decreased this proportion to 2% (Fig. 5 *C*, *F*, and *G*) ($P = 0.001$, $n = 4$ per group). Concomitant with this dramatic decrease in PanIN, the overall histological appearance of SAG21k-treated pancreata suggested a striking increase in stromal fibrosis (Fig. 5*C*). Interestingly, the remaining PanIN lesions in SAG21k-treated animals retained a ductal phenotype, marked by *Sox9* expression (see *Hh Pathway Modulation Affects Epithelial Progenitor Phenotype*), but displayed a change in shape from elongated tubular structures to closed globular masses (Fig. 5*F*).

To investigate whether proliferative differences in the epithelial compartment may account for these differences in PanIN abundance, we measured the incorporation of EdU into EpCAM$^+$ epithelial cells as a function of Hh-pathway modulation. We found in cerulein-treated KICG animals that EdU incorporation into EpCAM$^+$ cells varied from 2.5% with vehicle treatment to 7.5% in animals treated with vismodegib ($P = 0.0004$, $n = 5$ per group) to 1.0% in animals treated with SAG21k (Fig. 5 *D*, *E*, *F*, and *H*) ($P = 0.002$, $n = 5$ per group). These dramatic differences in proliferation parallel and likely account, at least in part, for the differences in PanIN abundance that accompany Hh pathway modulation.

Hh Pathway Modulation Affects Epithelial Progenitor Phenotype. Given the well-established developmental effect of Hh pathway activity on pancreatic progenitor cell phenotype, we examined the effects of pharmacologic Hh pathway modulation on progenitor phenotype in the pancreata of cerulein-treated KICG mice. In parallel with the increase in PanIN lesions caused by Hh signaling inhibition, we found that there was an increase in total numbers of Sox9$^+$ epithelial cells in response to vismodegib treatment and a decrease in response to SAG21k although the

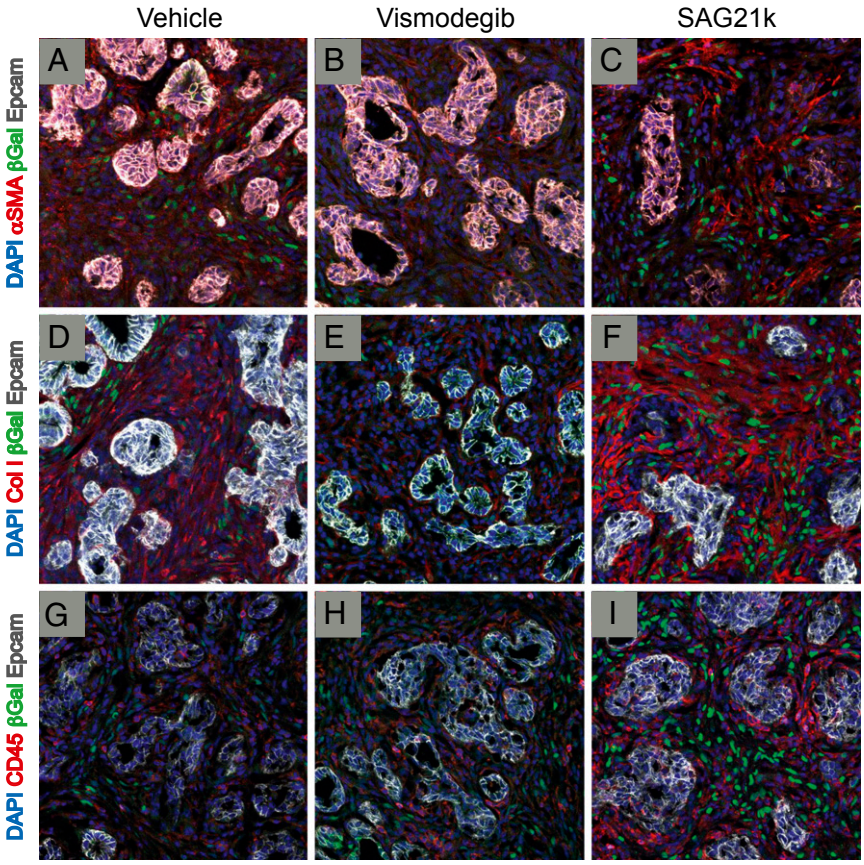

Fig. 4. Hh response regulates stromal composition during cerulein-enhanced oncogenesis. (*A–I*) Confocal images of pancreata of cerulein-treated KICG mice are shown. (*A* and *B*) Vismodegib decreased the expression of *αSMA*, an established marker for desmoplasia in PDA. (*C*) Conversely, SAG21k increased *αSMA* expression. (*D–F*) Expression of *Col I*, another marker for desmoplasia, was decreased by vismodegib and increased by SAG21k. (*G* and *H*) Pancreata from vehicle- and vismodegib-treated mice exhibit cells expressing *CD45*, suggestive of hematopoietic origin, dispersed in stromal areas between PanIN lesions. (*I*) In contrast, *CD45*$^+$ cells are concentrated around globular PanIN structures in SAG21k-treated mice. In all drug-treatment conditions shown, there is no overlap between *Gli1*$^+$ and *CD45*$^+$ cells.

proportion of PanIN epithelial was comparable with these mice irrespective of Hh pathway modulation (Fig. 6 *A–C*). Notably, Hh pathway activation dramatically reduced expression of Pdx1 to 0.2% of EpCAM$^+$ cells in SAG21K-treated mice compared with 7.0% or 8.5%, respectively, of EpCAM$^+$ cells in vehicle- or vismodegib-treated mice (Fig. 6 *D–G*) (vehicle vs. SAG21k, $P = 0.008$, $n = 6$ per group). As Pdx1 expression indicates progenitor cell character, we conclude that the proportion of cells with progenitor-like phenotype is slightly increased by Hh pathway inhibition but is dramatically reduced by Hh pathway activation. The doubling of PanIN lesion abundance associated with Hh pathway antagonism (Fig. 5*G*) thus likely results largely from differences in proliferative changes whereas the eight-fold reduction in PanIN lesions caused by pharmacologic Hh pathway activation is associated with both decreased progenitor-like character and decreased proliferation in the epithelial compartment.

Discussion

We have observed that genetic or pharmacologic inhibition of Hh pathway activity accelerates progression of oncogenic Kras-driven disease in three distinct murine models of PDA. Importantly, our study of the acute effects of pathway inhibition or activation highlighted a role for Hh pathway activity in controlling the balance between epithelial and stromal elements. Pathway activation thus causes stromal hyperplasia and reduced epithelial growth whereas pathway inhibition causes accelerated growth of epithelial elements and suppression of desmoplasia.

In pancreata of animals treated with SAG21k, the fibrotic appearance and augmented expression of αSMA and Col1 clearly show that pathway activation does not simply increase *Gli1* expression but actually increases desmoplastic character. The relative abundance of PanIN lesions also displays reciprocal changes in conjunction with Hh pathway inhibition and activation, and these changes parallel changes in proliferation and progenitor-cell character, both of which are suppressed by SAG21k-mediated pathway activation. Hh pathway activity indeed appears to suppress progenitor cell character whereas pathway inhibition increases the frequency of undifferentiated cells, as indicated, respectively, by reduced or increased expression of *Pdx1*; this effect has precedent in embryonic development, which requires the absence of Hh pathway activity for expression of *Pdx1* and normal development of the pancreatic rudiment (5–7). One other mechanism that may contribute to reduced abundance of PanIN is suggested by the appearance of presumed hematopoietic cells (CD45$^+$) in a zone around the globular epithelial structures, a behavior not observed in mice given either vehicle or vismodegib (Fig. 4 *G–I*). The functional significance of this margination is not understood, and these cells do not express markers of T-cell or macrophage fates (Fig. S4) but nevertheless may be involved in disposal of dead PanIN cells or play another role in reducing cellular proliferation and/or *Pdx1* expression.

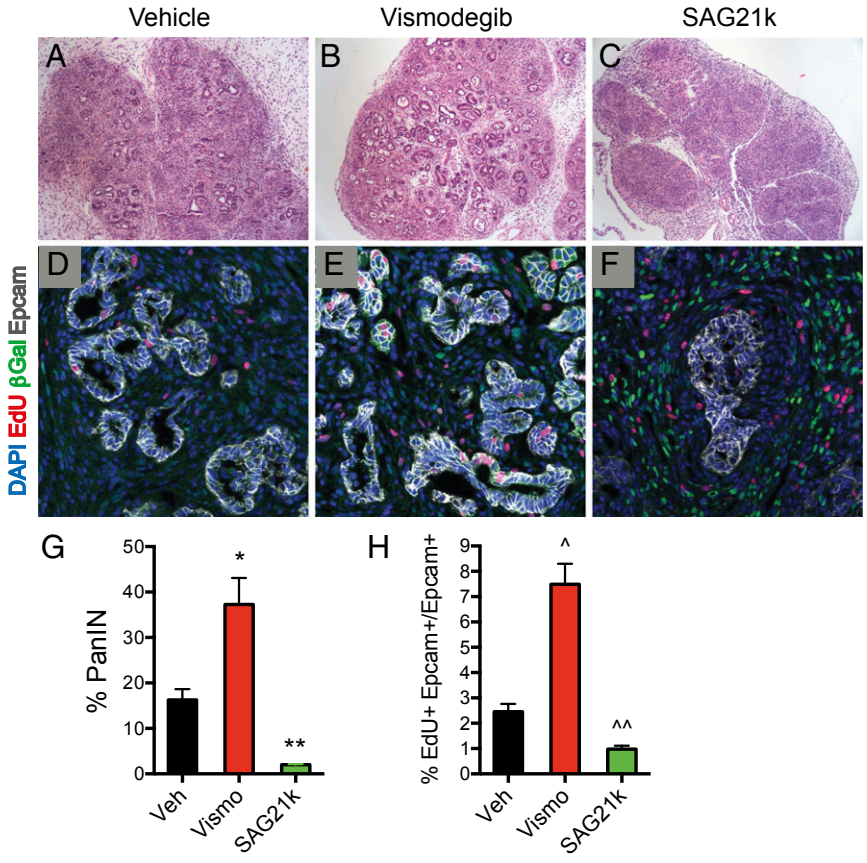

Fig. 5. Hh response suppresses PanIN formation and proliferation. (*A–C* and *G*) H&E sections of pancreata from KICG mice given cerulein show PanIN lesions. Vismodegib-treated mice showed 37% of the pancreas occupied by PanIN lesions compared with 16% for vehicle-treated controls (*$P = 0.016$, $n = 4$ each). In contrast, SAG21k-treated mice showed only 2% of the pancreas occupied by PanIN lesions along with increased overall fibrosis (**$P = 0.001$, vehicle vs. SAG21k, $n = 4$). Error bars indicate SEM. (*D–F* and *H*) Representative confocal images of PanIN lesions in pancreata of KICG mice are shown. Vismodegib increases the percentage of proliferating PanIN cells (EdU^+ $Epcam^+/Epcam^+$) to 7.5% compared with 2.5% for vehicle treatment (^$P = 0.0004$, $n = 5$ each). Conversely, SAG21k reduces proliferation percentage to 1.0% (^^$P = 0.002$, $n = 5$). Error bars indicate SEM.

Given that stromal cells are the primary site of Hh signal response, the dramatic effects of pathway activity on epithelial elements would seem to require stromal expression of secreted factors. Two studies have demonstrated that genetic ablation of Indian Hedgehog (Ihh) expression in the intestinal epithelium reduces stromal Hh response and leads to increased epithelial proliferation and decreased differentiation (43, 44). These studies have implicated decreased BMP signaling as the effector mechanism for increased epithelial proliferation. Further studies will be required to determine the role of Hh-inducible secreted stromal factors in the striking effects of Hh pathway activity that we have noted in the context of oncogenic Kras-driven disease.

We note that, although our studies clearly show acceleration of PDA progression with Hh pathway inhibition, several other lines of preclinical evidence have suggested that Hh pathway antagonists promote an antitumor response in PDA. Olive et al. (20) thus demonstrated that Hh antagonists decrease tumor desmoplasia and increase functional vascularity, allowing better tumor access of cytotoxic chemotherapy. This finding generated great initial enthusiasm for use of Hh antagonists in clinical trials for PDA. The results of these trials, however, have been either ambiguous or disappointing. Our study may provide a potential explanation for these clinical trial results because we observe that pharmacologic inhibition of Hh pathway activity also accelerates the formation and proliferation of PanINs and invasive PDA lesions. The ultimate outcome in clinical trials of Hh pathway antagonists combined with cytotoxic chemotherapy may thus depend on the balance of these opposing effects, with accelerated tumor growth counterbalancing the beneficial effect of enhanced cytotoxic drug access.

This balance between beneficial and harmful effects might be favorably influenced by the use of more potent cytotoxic agents, which, with better tumor access provided by decreased desmoplasia and increased microvasculature, could overcome the tumor-proliferative effects of Hh pathway antagonism. Indeed, although neither of two clinical trials combining an Hh antagonist with gemcitabine appeared to be effective, the more recent trial combining vismodegib with gemcitabine and nab-paclitaxel was potentially positive, possibly due to greater potency of the cytotoxic regimen. This principle may also help explain the positive results of previously published preclinical studies. The aforementioned work of Olive et al. (20) thus may have incorporated a level of gemcitabine sufficiently high as to benefit from the antidesmoplastic effect and consequent improved tumor access, thereby overcoming the tumor-proliferative effect of saridegib. In addition, the beneficial effect of cyclopamine treatment reported in an oncogenic Kras-driven model of PDA (13) may have been due to the combined cytotoxicity of cyclopamine above certain levels (12) alongside of its Hh pathway inhibitory effects. Future trials of Hh antagonists in combination with cytotoxic agents may benefit from selection of the most effective chemotherapy regimen possible, such as FOLFIRINOX (3).

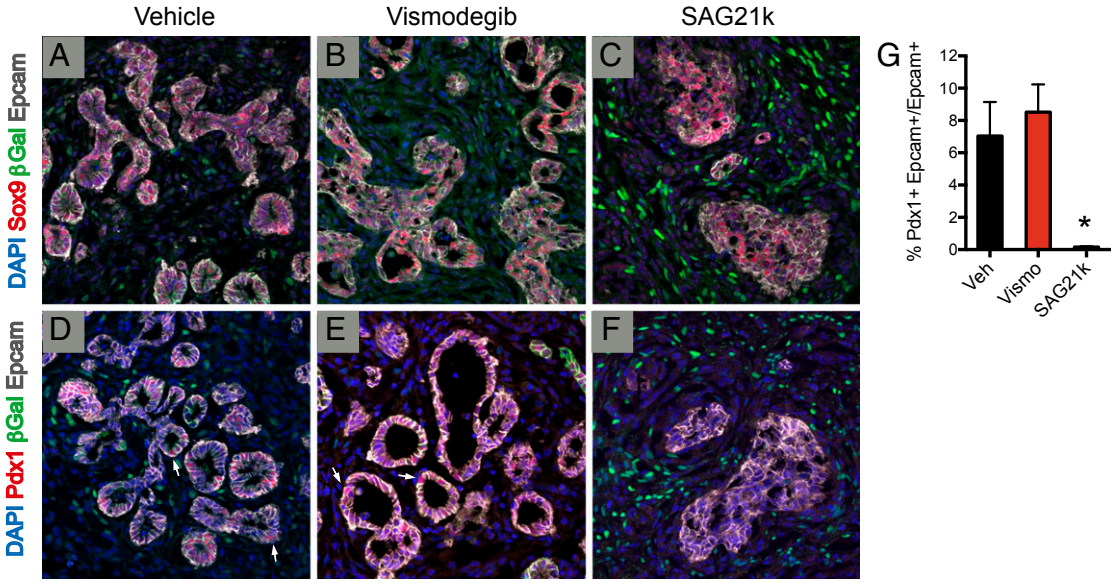

Fig. 6. Hh response suppresses expression of the pancreatic progenitor marker Pdx1 in PanIN lesions. (*A–C*) Confocal images of pancreata from KICG mice show nuclear expression of the ductal epithelial marker *Sox9* in all PanIN cells. Vismodegib or SAG21k does not alter expression in PanIN lesions. (*D–G*) In contrast, nuclear *Pdx1* expression is observed in a fraction of total PanIN cells in vehicle- and vismodegib-treated mice ($n = 6$ each), 7.0% and 8.5%, respectively. White arrows display *Pdx1* expression. Furthermore, SAG21k dramatically reduces *Pdx1* expression to 0.2% of PanIN cells (Vehicle vs. SAG21k, $*P = 0.008$, $n = 6$ each). Error bars indicate SEM.

Finally, although we have not examined the effect of Hh pathway activation on survival, our study suggests a potential therapeutic role for Hh pathway activation in PDA clinical trials. We have shown that SAG21k has antitumor activity, as it reduces proliferation of PanIN epithelial cells and reduces the *Pdx1*+ progenitor population. Pathway activation, however, also promotes desmoplasia, including increases in *Col I* and *αSMA* expression and hyperplasia of Hh-responsive fibroblasts. The use of an Hh pathway agonist in treatment of human disease thus may benefit from combination with additional agents that combat the reduced tumor access associated with desmoplasia (45, 46).

Materials and Methods

Mouse Strains and Histological Analysis. Mice were housed in pathogen-free animal facilities. All experiments were conducted under protocol 2005N000148 approved by the Subcommittee on Research Animal Care at Massachusetts General Hospital or under protocol 14605 approved by the Stanford Institutional Animal Care and Use Committee. Mice were maintained on mixed 129SV/C57BL/6 backgrounds. All mice included in the survival analysis were euthanized when criteria for disease burden were reached. The following mouse strains were used: *Ptfa1-Cre* (47), *LSL-KRAS^{G12D}* (48), *Shh$^{lox/lox}$* (49), *Trp53$^{lox/lox}$* (50), *Pdx1-Cre* (26), *Ink4a/Arf$^{-/-}$* (51), and *Gli1-nLacZ* (33). These strains were intercrossed to produce the experimental cohorts. For histopathologic analysis, pancreata were analyzed in blinded fashion by a single pathologist (V.D.) to determine the percent of each pancreas occupied by PanIN and PDA lesions.

In Vivo Ultrasound Imaging. Starting at 5 wk of age, pancreata of mice were imaged in the transverse and sagittal planes using 2D high-resolution brightness-mode (B-mode) imaging. A dedicated small animal ultrasound system was used (Vevo2100; spatial resolution, axial, 40 μm; lateral, 110 μm; 40-MHz MS-550D linear transducer; VisualSonics). A volume for each tumor focus was calculated as an ellipsoid using maximal length, width, and height measurements in millimeters: $\pi/6 \times (L \times W \times H)$. Volumes of individual foci were summed together for the total tumor volume per animal at each time of measurement.

Drug and Cerulein Treatments. Eight-week-old KC and KCS mice were injected with cerulein (Sigma) at a dose of 50 mcg/kg i.p. injection hourly × 6 on days 0 and 1. Mice were killed on day 30, and pancreata were harvested for histological examination and immunohistochemistry. Identical cerulein injection of ICG and KICG mice was conducted at 4 wk of age. Vehicle-treated mice received MCT (0.5% methylcellulose, 0.2% Tween 80) once daily at a volume of 10 μL/g of mouse weight. For vismodegib treatments, the compound was formulated in a 10-mg/mL suspension in MCT. SAG21k was formulated as a 0.5-mg/mL solution in MCT. Drug dosing was as follows: (*i*) The vismodegib treatment group received the compound at 100 mg/kg twice daily on days 0 and 1, and then once daily on days 2 through 8. The first dose of vismodegib immediately preceded the first injection of cerulein. (*ii*) The vehicle-treatment group received MCT vehicle on the same schedule as vismodegib treatment. (*iii*) The SAG21k treatment group received compound at 5 mg/kg oral gavage once daily on days 0 through 8. The first dose of SAG21k immediately preceded the first injection of cerulein. On day 8, mice were injected i.p. with 200 μL of 1 mg/mL EdU (5-ethynyl-2′-deoxyuridine; Invitrogen) in PBS, and then killed 2 h later with in vivo perfusion as described in *Histology and IHC*.

For survival studies and ultrasound scanning experiments, mice were given vismodegib (100 mg/kg) or vehicle once daily starting at the age of 5 wk.

For studies on uninjured animals described in Fig. S3, ICG or KICG animals were treated identically as described, in the absence of cerulein treatment.

Histology and IHC. To prevent autodigestion of the pancreas during tissue harvest, we performed in vivo tissue fixation. Animals were placed in deep anesthesia using isoflurane, and the animals were perfused with 20 mL of 4% paraformaldehyde/PBS [4% (wt/vol) PFA/PBS] injected through the left ventricle at a rate of 4 mL/min. Pancreata were excised and fixed overnight at 4 °C in 4% (wt/vol) PFA/PBS. Some of the fixed tissue was submitted for paraffin embedding, sectioning, and H&E staining (Histotec). For frozen sections, the fixed tissues were then transferred to 30% sucrose/PBS for 12–24 h, and then embedded into Optimal Cutting Temperature medium (OCT; Sakura Finetek).

Immunofluorescence staining was performed on 7-μm sections of fixed-frozen OCT-embedded samples. Primary antibodies used were as follows: chicken anti-beta galactosidase (ab616, 1:1,000; Abcam), rabbit anti-alpha smooth muscle actin (ab5694, 1:200; Abcam), anti-Epcam (clone G8.8 concentrated supernatant, 1:400; Developmental Studies Hybridoma Bank), rabbit anti-collagen I (ab21286, 1:250; Abcam), rat anti-CD45 (clone 30-F11, 1:100; Biolegend), rat anti-CD3 (clone 17A2, 1:200; Biolegend), rat anti-F4/80 (clone BM8, 1:200; Biolegend), rabbit anti-Pdx1 (Cat. no. 07–696, 1:400; Millipore), and rabbit anti-Sox9 (AB5535, 1:500; Millipore). EdU detection was performed with the Click-iT EdU Alexa 594 Imaging Kit (Invitrogen). Secondary antibodies used for visualization were from Jackson Immunoresearch or Sigma. Confocal microscopy was performed on a Zeiss LSM 700.

For immunohistochemistry, slides were deparaffinized in xylenes (two treatments, 6 min each), rehydrated sequentially in ethanol [5 min in 100%, 3 min in 95%, 3 min in 75%, and 3 min in 40% (vol/vol)], and washed for 5 min in 0.3% Triton X-100/PBS (PBST) and 3 min in water. For antigen unmasking, specimens were cooked in a 2100 Antigen Retriever (Aptum Biologics Ltd) in 1× Antigen Unmasking Solution, Citric Acid Based (H-3300; Vector Laboratories), rinsed three times with PBST, incubated for 10 min with 1% H_2O_2 at room temperature to block endogenous peroxidase activity, washed three times with PBST, and blocked with 5% goat serum in PBST for 1 h. Primary antibodies were diluted in blocking solution [anti-PCNA (1:200; Cell Signaling Technology) and anti-Sox9 (1:300; ab5535; Millipore)] and incubated with the tissue sections at 4 °C overnight. Specimens were then washed three times for 3 min each in PBST and incubated with biotinylated secondary antibody (Vector Laboratories) in blocking solution for 1 h at room temperature. Then, specimens were washed three times in PBST and treated with ABC reagent (ABC kit PK-6100; Vectastain) for 30 min, followed by three washes for 3 min each. Finally, slides were stained for peroxidase for 3 min with the DAB (Di-amine-benzidine) substrate kit (SK-4100; Vector Laboratories), washed with water, and counterstained with hematoxylin. Stained slides were photographed with an Olympus DP72 microscope. Images were processed using ImageJ and Adobe Photoshop CS4.

qRT-PCR. Freshly dissected pancreata were homogenized in TRIzol reagent (Invitrogen) using a hand-held motorized tissue homogenizer. Whole RNA was purified using the PureLink Mini Kit (Invitrogen) using standard protocols with on-column DNase digestion. cDNA was prepared using the SuperScript III First Strand Synthesis SuperMix (Invitrogen). qPCR was performed using iQ SYBR Green Supermix (Bio-Rad) with a Bio-Rad iCycler. Primers used were as follows: mouse Gli1 (mGli1F1, CCAAGCCAACTTTATGTCAGGG; mGli1R1, AGCCCGCTTCTTTGTTAATTTGA) and mouse HPRT1 (mHPRT1F1, TCAGTCAACGGGGGACATAAA; mHPRT1R1, GGGGCTGTACTGCTTAACCAG).

Statistical Analyses. Graphing and statistical analyses were performed with GraphPad Prism 6 software. Standard error measurements are presented in all quantified data unless otherwise specified. Paired data were analyzed with the unpaired *t* test. The log-rank test was used in Kaplan–Meier analyses.

Note. We note that two studies published while this work was under review independently arrived at similar conclusions: namely, that loss of Hh response in stromal cells (41) or ablation of stromal cells (42) can accelerate the progression of pancreatic cancer in oncogenic Kras based murine models.

ACKNOWLEDGMENTS. We thank Julien Sage for critical reading of the manuscript and members of the N.B. and P.A.B. laboratories for valuable input. N.B. holds the Gallagher Endowed Chair in Gastrointestinal Cancer Research at Massachusetts General Hospital and P.A.B. is the Ernest and Amelia Gallo Professor at the Stanford University School of Medicine. This work was supported by National Institutes of Health Grants R01CA133557-05, P01CA117969-07, and P50CA1270003 (to N.B.); 5R21CA158640-02 (to P.A.B. and J.K.W.); R01CA155289-01 (to J.K.W.); and R01CA136574 (to J.K.C.). This work was also supported by the Linda J. Verville Cancer Research Foundation (N.B.), a Seibel Scholar Fellowship (to J.J.L.), a Damon-Runyon Fellowship (to X.S.L.), and the Howard Hughes Medical Institute (P.A.B.). R.M.P. and N.B. are Andrew L. Warshaw Institute for Pancreatic Cancer Research Fellows.

1. Howlader N, et al. (2013) *SEER Cancer Statistics Review, 1975-2010* (National Cancer Institute, Rockville, MD).
2. Anonymous (2010) StatBite. U.S. pancreatic cancer rates. *J Natl Cancer Inst* 102(24):1822.
3. Conroy T, et al.; Groupe Tumeurs Digestives of Unicancer; PRODIGE Intergroup (2011) FOLFIRINOX versus gemcitabine for metastatic pancreatic cancer. *N Engl J Med* 364(19):1817–1825.
4. Von Hoff DD, et al. (2013) Increased survival in pancreatic cancer with nab-paclitaxel plus gemcitabine. *N Engl J Med* 369(18):1691–1703.
5. Hebrok M, Kim SK, Melton DA (1998) Notochord repression of endodermal Sonic hedgehog permits pancreas development. *Genes Dev* 12(11):1705–1713.
6. Hebrok M, Kim SK, St Jacques B, McMahon AP, Melton DA (2000) Regulation of pancreas development by hedgehog signaling. *Development* 127(22):4905–4913.
7. Kim SK, Melton DA (1998) Pancreas development is promoted by cyclopamine, a hedgehog signaling inhibitor. *Proc Natl Acad Sci USA* 95(22):13036–13041.
8. Strobel O, et al. (2010) Pancreatic duct glands are distinct ductal compartments that react to chronic injury and mediate Shh-induced metaplasia. *Gastroenterology* 138(3): 1166–1177.
9. Thayer SP, et al. (2003) Hedgehog is an early and late mediator of pancreatic cancer tumorigenesis. *Nature* 425(6960):851–856.
10. Hingorani SR, et al. (2005) Trp53R172H and KrasG12D cooperate to promote chromosomal instability and widely metastatic pancreatic ductal adenocarcinoma in mice. *Cancer Cell* 7(5):469–483.
11. Berman DM, et al. (2003) Widespread requirement for Hedgehog ligand stimulation in growth of digestive tract tumours. *Nature* 425(6960):846–851.
12. Yauch RL, et al. (2008) A paracrine requirement for hedgehog signalling in cancer. *Nature* 455(7211):406–410.
13. Feldmann G, et al. (2008) Hedgehog inhibition prolongs survival in a genetically engineered mouse model of pancreatic cancer. *Gut* 57(10):1420–1430.
14. Feldmann G, et al. (2007) Blockade of hedgehog signaling inhibits pancreatic cancer invasion and metastases: A new paradigm for combination therapy in solid cancers. *Cancer Res* 67(5):2187–2196.
15. Feldmann G, et al. (2008) An orally bioavailable small-molecule inhibitor of Hedgehog signaling inhibits tumor initiation and metastasis in pancreatic cancer. *Mol Cancer Ther* 7(9):2725–2735.
16. Bailey JM, Mohr AM, Hollingsworth MA (2009) Sonic hedgehog paracrine signaling regulates metastasis and lymphangiogenesis in pancreatic cancer. *Oncogene* 28(40): 3513–3525.
17. Tian H, et al. (2009) Hedgehog signaling is restricted to the stromal compartment during pancreatic carcinogenesis. *Proc Natl Acad Sci USA* 106(11):4254–4259.
18. Nolan-Stevaux O, et al. (2009) GLI1 is regulated through Smoothened-independent mechanisms in neoplastic pancreatic ducts and mediates PDAC cell survival and transformation. *Genes Dev* 23(1):24–36.
19. Bailey JM, et al. (2008) Sonic hedgehog promotes desmoplasia in pancreatic cancer. *Clin Cancer Res* 14(19):5995–6004.
20. Olive KP, et al. (2009) Inhibition of Hedgehog signaling enhances delivery of chemotherapy in a mouse model of pancreatic cancer. *Science* 324(5933):1457–1461.
21. Fendrich V, et al. (2011) Ectopic overexpression of Sonic Hedgehog (Shh) induces stromal expansion and metaplasia in the adult murine pancreas. *Neoplasia* 13(10): 923–930.
22. Rosow DE, et al. (2012) Sonic Hedgehog in pancreatic cancer: from bench to bedside, then back to the bench. *Surgery* 152(3, Suppl 1):S19–S32.
23. Anonymous (January 27, 2012) Press release: Infinity reports update from phase 2 study of saridegib plus gemcitabine in patients with metastatic pancreatic cancer. Available at www.businesswire.com/news/home/20120127005146/en/Infinity-Reports-Update-Phase-2-Study-Saridegib#.UxAvFfRdVxV. Accessed July 2, 2014.
24. Catenacci DVT, et al. (2012) A phase IB/randomized phase II study of gemcitabine (G) plus placebo (P) or vismodegib (V), a hedgehog (Hh) pathway inhibitor, in patients (pts) with metastatic pancreatic cancer (PC): Interim analysis of a University of Chicago phase II consortium study. *J Clin Oncol* 30(Suppl):Abstract 4022.
25. De Jesus-Acosta A, et al. (2014) A Phase II study of vismodegib, a hedgehog (Hh) pathway inhibitor, combined with gemcitabine and nab-paclitaxel (nab-P) in patients with untreated metastatic pancreatic ductal adenocarcinoma (PDA). *J Clin Oncol* 32(Suppl):257.
26. Hingorani SR, et al. (2003) Preinvasive and invasive ductal pancreatic cancer and its early detection in the mouse. *Cancer Cell* 4(6):437–450.
27. Jensen JN, et al. (2005) Recapitulation of elements of embryonic development in adult mouse pancreatic regeneration. *Gastroenterology* 128(3):728–741.
28. Kopp JL, et al. (2012) Identification of Sox9-dependent acinar-to-ductal reprogramming as the principal mechanism for initiation of pancreatic ductal adenocarcinoma. *Cancer Cell* 22(6):737–750.
29. Guerra C, et al. (2007) Chronic pancreatitis is essential for induction of pancreatic ductal adenocarcinoma by K-Ras oncogenes in adult mice. *Cancer Cell* 11(3):291–302.
30. Fendrich V, et al. (2008) Hedgehog signaling is required for effective regeneration of exocrine pancreas. *Gastroenterology* 135(2):621–631.
31. Apelqvist A, Ahlgren U, Edlund H (1997) Sonic hedgehog directs specialised mesoderm differentiation in the intestine and pancreas. *Curr Biol* 7(10):801–804.
32. Aguirre AJ, et al. (2003) Activated Kras and Ink4a/Arf deficiency cooperate to produce metastatic pancreatic ductal adenocarcinoma. *Genes Dev* 17(24):3112–3126.
33. Bai CB, Auerbach W, Lee JS, Stephen D, Joyner AL (2002) Gli2, but not Gli1, is required for initial Shh signaling and ectopic activation of the Shh pathway. *Development* 129(20):4753–4761.
34. Sastra SA, Olive KP (2013) Quantification of murine pancreatic tumors by high-resolution ultrasound. *Methods Mol Biol* 980:249–266.
35. Foygel K, et al. (2013) Detection of pancreatic ductal adenocarcinoma in mice by ultrasound imaging of thymocyte differentiation antigen 1. *Gastroenterology* 145(4): 885–894, e3.
36. Brunton SA, et al. (2009) Potent agonists of the Hedgehog signaling pathway. *Bioorg Med Chem Lett* 19(15):4308–4311.
37. Whatcott CJ, Posner RG, Von Hoff DD, Han H (2012) Desmoplasia and chemoresistance in pancreatic cancer. *Pancreatic Cancer and Tumor Microenvironment*, eds Grippo PJ, Munshi HG (Transworld Research Network, Trivandrum, India).
38. Apte MV, et al. (2004) Desmoplastic reaction in pancreatic cancer: Role of pancreatic stellate cells. *Pancreas* 29(3):179–187.
39. Mollenhauer J, Roether I, Kern HF (1987) Distribution of extracellular matrix proteins in pancreatic ductal adenocarcinoma and its influence on tumor cell proliferation in vitro. *Pancreas* 2(1):14–24.
40. Imamura T, et al. (1995) Quantitative analysis of collagen and collagen subtypes I, III, and V in human pancreatic cancer, tumor-associated chronic pancreatitis, and alcoholic chronic pancreatitis. *Pancreas* 11(4):357–364.
41. Rhim AD, et al. (2014) Stromal elements act to restrain, rather than support, pancreatic ductal adenocarcinoma. *Cancer Cell* 25(6):735–747.

42. Ozdemir BC, et al. (2014) Depletion of carcinoma-associated fibroblasts and fibrosis induces immunosuppression and accelerates pancreas cancer with reduced survival. *Cancer Cell* 25(6):719–734.
43. Kosinski C, et al. (2010) Indian hedgehog regulates intestinal stem cell fate through epithelial-mesenchymal interactions during development. *Gastroenterology* 139(3): 893–903.
44. van Dop WA, et al. (2010) Loss of Indian Hedgehog activates multiple aspects of a wound healing response in the mouse intestine. *Gastroenterology* 139(5):1665–1676, e1–e10.
45. Provenzano PP, et al. (2012) Enzymatic targeting of the stroma ablates physical barriers to treatment of pancreatic ductal adenocarcinoma. *Cancer Cell* 21(3): 418–429.
46. Provenzano PP, Hingorani SR (2013) Hyaluronan, fluid pressure, and stromal resistance in pancreas cancer. *Br J Cancer* 108(1):1–8.
47. Kawaguchi Y, et al. (2002) The role of the transcriptional regulator Ptf1a in converting intestinal to pancreatic progenitors. *Nat Genet* 32(1):128–134.
48. Jackson EL, et al. (2001) Analysis of lung tumor initiation and progression using conditional expression of oncogenic K-ras. *Genes Dev* 15(24):3243–3248.
49. Lewis PM, et al. (2001) Cholesterol modification of sonic hedgehog is required for long-range signaling activity and effective modulation of signaling by Ptc1. *Cell* 105(5):599–612.
50. Jonkers J, et al. (2001) Synergistic tumor suppressor activity of BRCA2 and p53 in a conditional mouse model for breast cancer. *Nat Genet* 29(4):418–425.
51. Serrano M, et al. (1996) Role of the INK4a locus in tumor suppression and cell mortality. *Cell* 85(1):27–37.

Supporting Information

Lee et al. 10.1073/pnas.1411679111

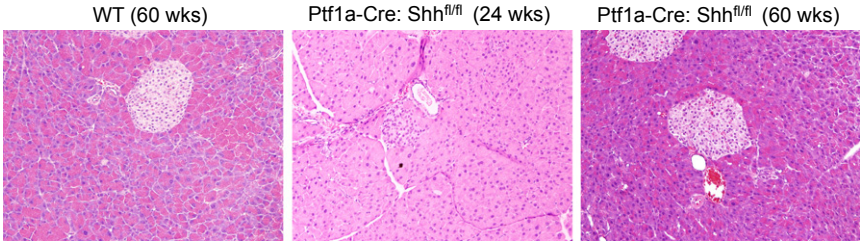

Fig. S1. Deletion of Shh is dispensable for normal pancreas development. Representative histology of pancreata from a 60-wk-old wild-type mouse (*Left*), 24-wk-old *Ptf1a-Cre:Shh$^{fl/fl}$* mouse (*Center*), and 60-wk-old *Ptf1a-Cre:Shh$^{fl/fl}$* mouse (*Right*).

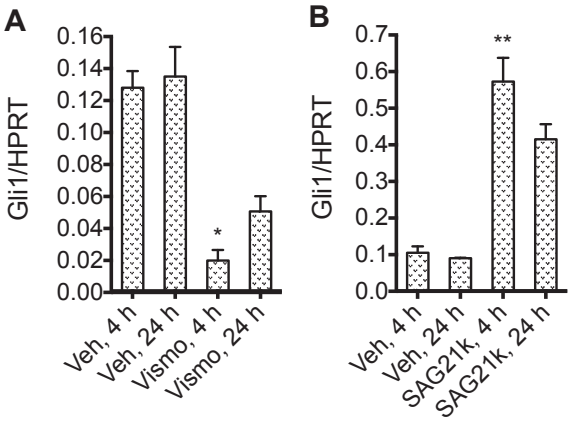

Fig. S2. Pharmacologic modulation of Hh pathway response in mice. (*A*) Normalized *Gli1* expression in pancreata of 9-wk-old male FVB mice given either MCT vehicle ($n = 3$) or vismodegib at 100 mg/kg ($n = 3$) by oral gavage daily for 5 d. Pancreata were harvested either 4 h or 24 h after the last dose of drug as shown. A 6.4-fold relative reduction of *Gli1* expression was observed in vismodegib-treated mice (Veh 4 h vs. Vismo 4 h, $*P = 0.0001$). (*B*) Normalized *Gli1* expression in pancreata of 9-wk-old male FVB mice given either MCT vehicle ($n = 3$) or SAG21k at 5 mg/kg ($n = 3$) by oral gavage daily for 5 d. Pancreata were harvested either 4 h or 24 h after the last dose of drug as shown. A 5.5-fold relative increase in *Gli1* expression was observed in SAG21k-treated mice (Veh 4 h vs. SAG21k 4 h, $**P = 0.002$). Error bars indicate SEM.

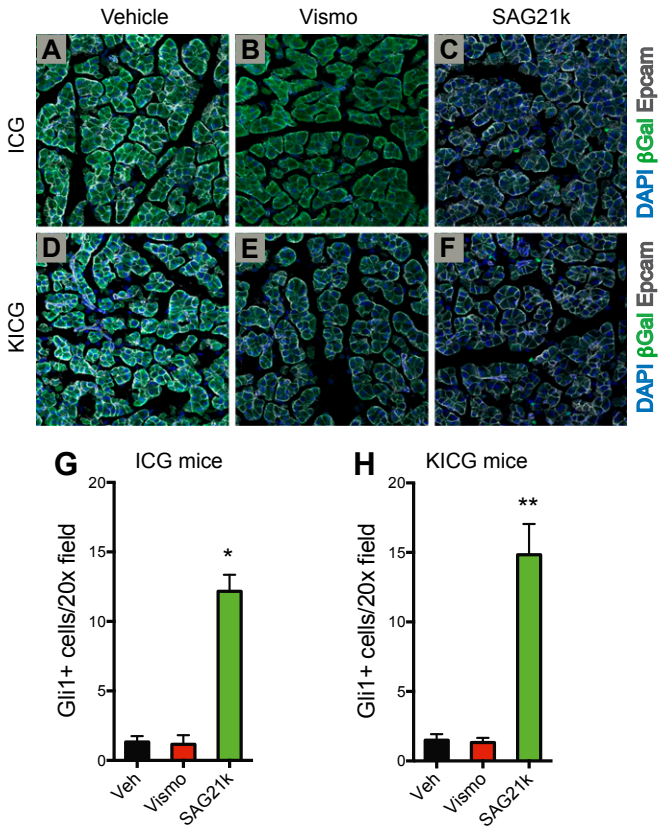

Fig. S3. Modulation of Hh response without concomitant cerulein controls the number of *Gli*$^+$ cells in pancreata. (*A–C* and *G*) ICG mice were treated as in Fig. 4, except that cerulein was not administered. Vismodegib does not alter significantly the number of *Gli1*$^+$ cells. However, SAG21k increases the number of *Gli1*$^+$ cells by 9.1-fold (*$P < 0.0001$, $n = 6$). Error bars indicate SEM. (*D–F* and *H*) KICG mice were similarly examined. Likewise, vismodegib does not alter the number of *Gli1*$^+$ cells whereas SAG21k increases the number by 9.9-fold (**$P < 0.0001$, $n = 6$). Error bars indicate SEM.

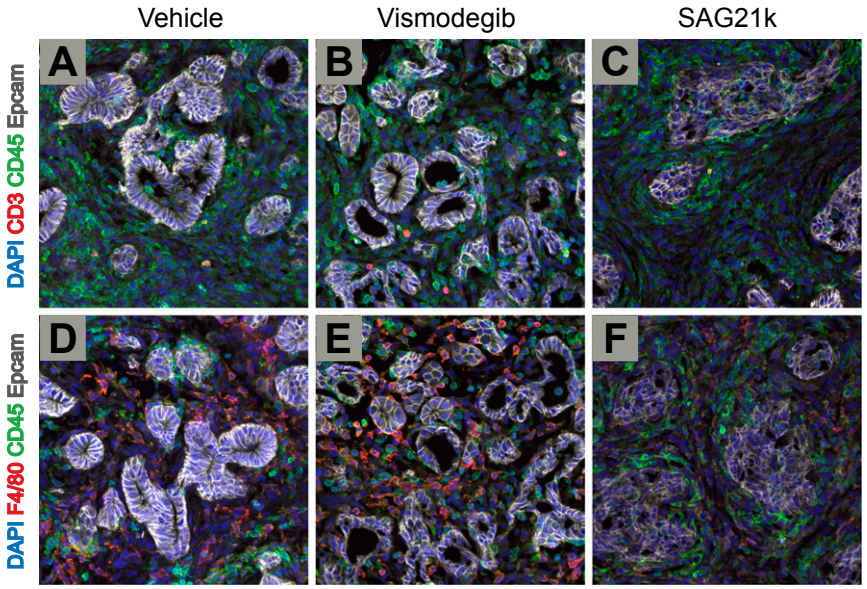

Fig. S4. Identity of CD45-positive hematopoietic cells during cerulein-enhanced oncogenesis. (*A–F*) Confocal images of pancreata of cerulein-treated KICG mice are shown. (*A–C*) CD3$^+$ T cells (orange or yellow) represent a minor fraction of the CD45$^+$ inflammatory infiltrate in vehicle-, vismodegib-, and SAG21k-treated mice. (*D–F*) F4/80$^+$ macrophages (orange or yellow) also represent a fraction of CD45$^+$ cells but appear more prevalent than CD3$^+$ cells under all three treatment conditions. (*C* and *F*) Notably, the zone of CD45$^+$ cells around globular epithelial structures in SAG21k-treated mice does not contain a predominance of either CD3$^+$ or F4/80$^+$ cells.